

LETTER • OPEN ACCESS

## Global wetland contribution to 2000–2012 atmospheric methane growth rate dynamics

To cite this article: Benjamin Poulter *et al* 2017 *Environ. Res. Lett.* **12** 094013

View the [article online](#) for updates and enhancements.

### Related content

- [Attribution of changes in global wetland methane emissions from pre-industrial to present using CLM4.5-BGC](#)  
Rajendra Paudel, Natalie M Mahowald, Peter G M Hess et al.
- [Surface water inundation in the boreal-Arctic: potential impacts on regional methane emissions](#)  
Jennifer D Watts, John S Kimball, Annett Bartsch et al.
- [Influence of changes in wetland inundation extent on net fluxes of carbon dioxide and methane in northern high latitudes from 1993 to 2004](#)  
Qianlai Zhuang, Xudong Zhu, Yujie He et al.

## Environmental Research Letters



## LETTER

## Global wetland contribution to 2000–2012 atmospheric methane growth rate dynamics

## OPEN ACCESS

## RECEIVED

1 December 2016

## REVISED

25 June 2017

## ACCEPTED FOR PUBLICATION

2 August 2017






## PUBLISHED

13 September 2017

Original content from this work may be used under the terms of the [Creative Commons Attribution 3.0 licence](#).

Any further distribution of this work must maintain attribution to the author(s) and the title of the work, journal citation and DOI.



Benjamin Poulter<sup>1,2,21</sup>, Philippe Bousquet<sup>3</sup>, Josep G Canadell<sup>4</sup>, Philippe Ciais<sup>3</sup>, Anna Peregon<sup>3</sup>, Marielle Saunois<sup>3</sup>, Vivek K Arora<sup>5</sup>, David J Beerling<sup>6</sup>, Victor Brovkin<sup>7</sup>, Chris D Jones<sup>8</sup>, Fortunat Joos<sup>9</sup>, Nicola Gedney<sup>19</sup>, Akihito Ito<sup>10</sup>, Thomas Kleinen<sup>7</sup>, Charles D Koven<sup>11</sup>, Kyle McDonald<sup>12</sup>, Joe R Melton<sup>5</sup>, Changhui Peng<sup>13</sup>, Shushi Peng<sup>3</sup>, Catherine Prigent<sup>14</sup>, Ronny Schroeder<sup>15</sup>, William J Riley<sup>11</sup>, Makoto Saito<sup>10</sup>, Renato Spahni<sup>9</sup>, Hanqin Tian<sup>16</sup>, Lyla Taylor<sup>6</sup>, Nicolas Viovy<sup>3</sup>, David Wilton<sup>6</sup>, Andy Wiltshire<sup>8</sup>, Xiyan Xu<sup>11,20</sup>, Bowen Zhang<sup>16</sup>, Zhen Zhang<sup>2,17</sup> and Qian Zhu<sup>18</sup>

<sup>1</sup> NASA Goddard Space Flight Center, Biospheric Sciences Laboratory, Greenbelt, MD 20771, United States of America

<sup>2</sup> Institute on Ecosystems and Department of Ecology, Montana State University, Bozeman, MT 59717, United States of America

<sup>3</sup> Laboratoire des Sciences du Climat et de l'Environnement, LSCE-IPSL (CEA-CNRS-UVSQ), 91191 Gif-sur-Yvette, France

<sup>4</sup> Global Carbon Project, CSIRO Marine and Atmospheric Research Oceans and Atmosphere, Canberra, ACT 2601, Australia

<sup>5</sup> Climate Research Division Environment Canada, Victoria, BC, V8W 2Y2, Canada

<sup>6</sup> Department of Animal and Plant Sciences, University of Sheffield, Sheffield S10 2TN, United Kingdom

<sup>7</sup> Max Planck Institute for Meteorology, Bundesstrasse 53, 20146 Hamburg, Germany

<sup>8</sup> Met Office Hadley Centre, FitzRoy Road, Exeter, EX1 3PB, United Kingdom

<sup>9</sup> Climate and Environmental Physics, Physics Institute & Oeschger Centre for Climate Change Research, University of Bern, Switzerland

<sup>10</sup> Center for Global Environmental Research, National Institute for Environmental Studies, Tsukuba, Japan

<sup>11</sup> Climate & Ecosystem Sciences Division, Lawrence Berkeley National Lab, 1 Cyclotron Road, Berkeley, CA 94720, United States of America

<sup>12</sup> Department of Earth and Atmospheric Sciences, City University of New York, New York, NY 10031, United States of America

<sup>13</sup> Department of Biology Sciences, Institute of Environment Science, University of Quebec at Montreal, Montreal, QC H3C 3P8, Canada

<sup>14</sup> CNRS/LERMA, Observatoire de Paris, 61 Ave. de l'Observatoire, 75014 Paris, France

<sup>15</sup> Department of Civil & Environmental Engineering, University of New Hampshire, Durham, NH 03824, United States of America

<sup>16</sup> International Center for Climate and Global Change Research and School of Forestry and Wildlife Sciences, Auburn University, Auburn, AL 36849, United States of America

<sup>17</sup> Swiss Federal Research Institute WSL, Birmensdorf 8059, Switzerland

<sup>18</sup> State Key Laboratory of Soil Erosion and Dryland Farming on the Loess Plateau, Northwest A&F University, Yangling 712100, People's Republic of China

<sup>19</sup> Met Office Hadley Centre, Joint Centre for Hydrometeorological Research, Maclean Building, Wallingford OX10 8BB, United Kingdom

<sup>20</sup> Key Laboratory of Regional Climate-Environment for Temperate East Asia, Institute of Atmospheric Physics, Chinese Academy of Sciences, Beijing 100029, People's Republic of China

<sup>21</sup> Author to whom any correspondence should be addressed

E-mail: [benjamin.poulter@nasa.gov](mailto:benjamin.poulter@nasa.gov)

**Keywords:** methanogenesis, wetlands, methane

Supplementary material for this article is available [online](#)

**Abstract**

Increasing atmospheric methane (CH<sub>4</sub>) concentrations have contributed to approximately 20% of anthropogenic climate change. Despite the importance of CH<sub>4</sub> as a greenhouse gas, its atmospheric growth rate and dynamics over the past two decades, which include a stabilization period (1999–2006), followed by renewed growth starting in 2007, remain poorly understood. We provide an updated estimate of CH<sub>4</sub> emissions from wetlands, the largest natural global CH<sub>4</sub> source, for 2000–2012 using an ensemble of biogeochemical models constrained with remote sensing surface inundation and inventory-based wetland area data. Between 2000–2012, boreal wetland CH<sub>4</sub> emissions increased by 1.2 Tg yr<sup>-1</sup> (–0.2–3.5 Tg yr<sup>-1</sup>), tropical emissions decreased by 0.9 Tg yr<sup>-1</sup> (–3.2–1.1 Tg yr<sup>-1</sup>), yet globally, emissions remained unchanged at 184 ± 22 Tg yr<sup>-1</sup>. Changing air temperature was responsible for increasing high-latitude emissions whereas declines in low-latitude wetland area decreased tropical emissions; both dynamics are consistent with features of predicted centennial-scale climate change impacts on wetland CH<sub>4</sub> emissions. Despite uncertainties in wetland area mapping, our study shows that global wetland CH<sub>4</sub> emissions have not contributed significantly to the period of renewed atmospheric CH<sub>4</sub> growth, and is consistent with findings from studies that indicate some combination of increasing fossil fuel and agriculture-related CH<sub>4</sub> emissions, and a decrease in the atmospheric oxidative sink.

## Introduction

The increase of methane ( $\text{CH}_4$ ) in the atmosphere is responsible for approximately 20% of the radiative forcing related to contemporary climate change (Ciais *et al* 2013). Since 1850, atmospheric  $\text{CH}_4$  concentrations have risen by more than 150%, from a pre-industrial level of 700 ppb to 1834 ppb in 2015, primarily as a result of human activities that include fossil fuel extraction and agriculture practices (Kirschke *et al* 2013, Ruddiman 2013, Dlugokencky *et al* 2015, Tian *et al* 2016). In recent assessments of the global  $\text{CH}_4$  budget, covering the period 1980 to 2009, natural wetlands were estimated to be the largest but also most uncertain source of  $\text{CH}_4$ , emitting between 177–284 Tg  $\text{CH}_4 \text{ yr}^{-1}$  using bottom-up modeling approaches and 142–208 Tg  $\text{CH}_4 \text{ yr}^{-1}$  based on top-down atmospheric inversions (Kirschke *et al* 2013). Wetland emissions now represent about 30% of the total combined natural and anthropogenic sources and are projected to increase and amplify global warming (Stocker *et al* 2013). The large differences among published source estimates results from difficulties in defining wetland  $\text{CH}_4$  producing area, uncertainties in biogeochemical modeling of anaerobic sources, oxidative sinks, and from uncertainties in atmospheric inversions (Melton *et al* 2013, Wania *et al* 2013, Patra *et al* 2016).

The atmospheric growth rate of  $\text{CH}_4$  exhibits complex temporal variability, because (1) the gas has a short perturbation lifetime,  $\sim 12$  years (Prather *et al* 2012), compared to longer-lived gases such as  $\text{CO}_2$  for which emissions accumulate in the atmosphere on centennial to millennial timescales (Ciais *et al* 2013), and (2) the sources and sinks are diverse and can change rapidly over short time periods (Dlugokencky *et al* 1999, Bousquet *et al* 2006). For example, atmospheric  $\text{CH}_4$  concentrations increased by approximately  $12 \pm 6 \text{ ppb yr}^{-1}$  during the 1980s (based on observations made by the National Oceanic and Atmospheric Administration's (NOAA) Earth System Research Laboratory (ESRL) at the Mauna Loa Observatory, MLO); however in the 1990s a slowdown in growth was observed (Dlugokencky *et al* 1999), followed by a stabilization in the atmospheric growth rate of  $\text{CH}_4$  that began in 1999 and lasted until 2006 (Dlugokencky *et al* 2009). Starting in 2007 and continuing to 2015, atmospheric  $\text{CH}_4$  concentrations began to increase once more, at an average rate of  $6.4 \text{ ppb yr}^{-1}$ , equivalent to  $17.8 \text{ Tg yr}^{-1}$ , (Dlugokencky *et al* 2015). The drivers responsible for the  $\text{CH}_4$  stabilization period remain unclear and may be due to changes in the concentration of atmospheric hydroxyl (OH) radicals, the main oxidative sink for methane (Heimann 2011), but with isotopic evidence also supporting either a reduced contribution from fossil fuel emissions (Aydin *et al* 2011), or reduced emissions from natural wetlands and rice cultivation (Kai *et al* 2011). In contrast, the period of renewed atmospheric  $\text{CH}_4$  growth

shows high latitudinal variability (Nisbet *et al* 2014), and several explanations have been proposed, including a reduction in the OH sink capacity for  $\text{CH}_4$  (Rigby *et al* 2008), increases in Arctic and tropical wetland emissions (Dlugokencky *et al* 2009), increased fossil fuel activities related to hydraulic fracking and natural gas exploitation (Jackson *et al* 2014, Rice *et al* 2016, Turner *et al* 2016), and possible changes in agriculture, in particular livestock production (Herrero *et al* 2013). Recent observational evidence suggests that the depletion of atmospheric  $\delta^{13}\text{C}$  of  $\text{CH}_4$  since 2007 supports a storyline for increasing biogenic emissions from agriculture (Schaefer *et al* 2016) rather than a decreasing thermogenic (fossil fuel related) or pyrogenic (biomass burning) emissions (Ghosh *et al* 2015).

The role of natural wetlands in the periods of stabilization (1999–2006) and renewed growth (2007–2012) has generally been overlooked in recent global  $\text{CH}_4$  budgets because these assessments have ended too early, i.e. 1993–2004 in the WETCHIMP ecosystem model ensemble (Melton *et al* 2013), 1980–2009 in the Kirschke *et al* (2013) study, and up to 2008 in the Dlugokencky *et al* (2009) study. An additional constraint has been the limited availability and scope of temporal wetland dynamics datasets, such as the Global Inundation Extent from Multi-Satellites Observations (GIEMS), which presently only covers 1993 to 2007 (Prigent *et al* 2007, Papa *et al* 2010) and excludes seasonal or permanent wetlands where surface inundation, or flooding, is not observed. Because a key requirement for wetlands to produce  $\text{CH}_4$  is by anaerobic soil respiration, where saturated or flooded soil conditions limit oxygen availability and thus create a suitable environment for methanogenesis, the accurate mapping of wetland area is critically important for estimating emissions. We address this issue, and problems related to comprehensively mapping wetland types (Adam *et al* 2010, Bohn *et al* 2015), by merging dynamic satellite remote sensing data of surface inundation for the 2000–2012 period (Schroeder *et al* 2015) with a static inventory of wetlands (Lehner and Doll 2004) following the same definition for natural wetlands used in Matthews and Fung (1987) and Melton *et al* (2013). These wetland definitions include both permanently and seasonally flooded soils, and include soils with either surface inundation or sub-surface saturation or both. Our definition includes only natural freshwater wetlands that are vegetated, such as peatland systems (bogs and fens) and mineral wetlands (including swamps and marshes), and attempts to avoid double counting of wetland emissions by excluding lakes, rivers, rice cultivation, saline estuaries, salt marshes, and reservoirs, which are typically accounted for as separate  $\text{CH}_4$  fluxes in global inventories (Saunio *et al* 2016).

An additional challenge in wetland  $\text{CH}_4$  emission modeling is that multiple pathways for  $\text{CH}_4$  production, consumption, and release exist within

wetlands; anaerobically produced  $\text{CH}_4$  is released to the atmosphere after being affected by a combination of processes that include oxidation by methanotrophic bacteria in the soil before diffusion to the atmosphere via plant transport structures known as ‘aerenchyma’, ebullition or through soil pores. Wetland models represent these biogeochemical and biophysical processes with varying degrees of complexity, with some modeling approaches estimating only the net flux of  $\text{CH}_4$  as a ratio of  $\text{CO}_2$  to  $\text{CH}_4$  production (Christensen *et al* 1996, Kaplan 2002) and other approaches representing multiple individual processes involved in the production, consumption, and transport of  $\text{CH}_4$  to the atmosphere (Cao *et al* 1996, Walter *et al* 2001, Riley *et al* 2011, Zürcher *et al* 2013, Grant *et al* 2015). The various formulations of model structure, parameterization, and initialization lead to relatively high uncertainties and emphasize the need for an ensemble approach in any comprehensive evaluation of the temporal dynamics and long-term evolution of global wetland  $\text{CH}_4$  emissions. The use of multiple biogeochemical models also allows for testing hypotheses related to either the climatic sensitivity of methane emissions, versus wetland area, or substrate limitation, for example.

To extend the record of observations, and to consider process-based uncertainties, an ensemble of eleven biogeochemical models that simulate  $\text{CH}_4$  emissions followed a common protocol (see Methods) to provide monthly integrated global wetland  $\text{CH}_4$  emissions at  $0.5^\circ$  spatial resolution from 2000–2012. Global wetland area and inundation dynamics were estimated by merging (see Methods) remote sensing based observations of daily surface inundation from the Surface Water Microwave Product Series (SWAMPS; Schroeder *et al* 2015) with the static inventory of wetland area from the Global Lakes and Wetlands Database (GLWD; Lehner and Doll 2004). This approach aimed to reduce uncertainties in wetland area estimation using prognostic approaches (Melton *et al* 2013) and also addressed known issues associated with remote sensing of surface inundation where sub-surface saturation and forested wetlands are poorly detected (Bohn *et al* 2015). Methane emissions from lakes and rice paddies (Zhang *et al* 2016a), and soil consumption of atmospheric  $\text{CH}_4$  (Curry 2007) are excluded from our estimates and included in more a recent multi-sectorial analysis of the global  $\text{CH}_4$  budget (Saunio *et al* 2016). The overall objectives of this study were to (i) provide an estimate up to 2012 for global wetland  $\text{CH}_4$  emissions, (ii) quantify the role of wetlands  $\text{CH}_4$  emissions on the stabilization period (2000–2006) and the renewed growth period (2007–2012), and (iii) partition the relative role of meteorological drivers, their teleconnections, and wetland area dynamics on wetland  $\text{CH}_4$  emissions between 2000–2012.

## Methods

### Wetland area dynamics

To reduce the uncertainty for wetland area dynamics resulting from predictive modeling approaches such as TOPMODEL (Gedney and Cox 2003), we combined remote sensing and inventory data to develop a monthly global wetland area dataset. Current satellite remote sensing of wetlands uses coarse-spatial resolution passive and active microwave sensors,  $\sim 25 \text{ km}^2$ , that observe surface water generally not obscured by vegetation (Bohn *et al* 2015, Schroeder *et al* 2015). This includes open water (e.g. lakes, rivers and ocean) as well as surface inundated wetlands comprising mainly of open plant canopies, and thus excludes exposed wetlands with no observable surface flooding as well as surface inundated wetlands beneath closed (forest) canopies. Consequently, whereas ground-based wetland inventories estimate between 8.2 and 10.1  $\text{Mkm}^2$  of wetlands globally (Lehner and Doll 2004), remote sensing surface water estimates of wetlands are far lower, i.e.  $\sim 6.5 \text{ Mkm}^2$  excluding coastal grid regions (Schroeder *et al* 2015). To develop a comprehensive wetland dynamics dataset, we integrated the Global Lakes and Wetlands Dataset, or GLWD (Lehner and Doll 2004), with the seasonal cycle of surface water inundation from the Surface Water Microwave Product Series (SWAMPS; Schroeder *et al* 2015).

The SWAMPS dataset maps fractional surface water dynamics using remote sensing data from multiple passive and active microwave satellite missions using a 28 day screening procedure to mask snow, ice cover, and melting snow. In our analysis, SWAMPS surface inundation was derived from the Special Sensor Microwave Imager version 1 and 2 (SSM/I v1/v2), SeaWinds-on-QuickSCAT (QSCAT) from January 2000 to October 2008, and from the European Space Agency Advanced Scatterometer (ASCAT) from November 2008 to December 2012. Land-cover data from MOD12Q1 V004 (Friedl *et al* 2010) was used to exclude permanent open water (water bodies, rivers, snow/ice) and thus avoid double counting of wetlands, with an additional global FAO land mask (Zobler 1986) applied to remove coastal grid cells where brackish and salt-water wetlands were not considered as a source of methane. The monthly SWAMPS dataset (‘fw\_28\_swe’) was re-projected from its native  $0.25^\circ$  EASE grid to a geographic  $0.5^\circ$  rectilinear grid (WGS84) using a conservative remapping interpolation to preserve the original wetland area.

The GLWD Level 3 dataset was first reclassified to remove Classes 1–3, lakes, reservoirs and rivers, and then aggregated by summing wetland area to  $0.5^\circ$  from 30 arc-second resolution. GLWD is commonly used as a benchmark for various remote sensing and wetland mapping activities because it incorporates

the highest-quality country-level inventory coverage of wetlands (Peregon *et al* 2008, Fluet-Chouinard *et al* 2014, Bohn *et al* 2015). The integration of SWAMPS and GLWD took place in three phases; first the maximum annual surface water fraction at the per-pixel level ( $FwMax_{x,y}$ ) for the 2000–2012 period was compared with GLWD ( $GLWD_{max_{x,y}}$ ) to estimate the relative SWAMPS detection bias ( $FwMaxCor_{x,y}$ ).

$$FwMaxCor_{x,y} = \frac{GLWD_{x,y}}{FwMax_{x,y}} \quad (1)$$

Second,  $FwMax_{x,y}$  from SWAMPS was adjusted using the  $FwMaxCor_{x,y}$  correction factor from equation (1) so that the maximum surface-water fraction from SWAMPS matched the GLWD estimate equation (2). For areas approximately northwest of the Hudson Bay Lowlands, the GLWD classifies the entire region as ‘lakes’, and so in cases where the merging SWAMPS-GLWD resulted in lower wetland area, the original SWAMPS surface-water values were used equation (3). Seasonal wetlands in desert systems, mapped in the GLWD, were retained in the SWAMPS-GLWD product.

$$FwMaxGLWD_{x,y} = FwMaxCor_{x,y} FwMax_{x,y} \quad (2)$$

$$FwMaxGLWD_{x,y} = \text{if } (FwMaxGLWD_{x,y} < FwMax_{x,y}, FwMax_{x,y}) \quad (3)$$

Third, the original monthly SWAMPS surface-inundation ( $Fw_{x,y,m}$ ) was rescaled equation (4) for each year as a fraction of that same year’s (uncorrected) maximum inundation, resulting in a unique monthly scalar (0–1) for each year ( $FwScalar_{x,y,m}$ ). Lastly,  $FwMaxCor_{x,y}$  was multiplied by the annual fractional inundation cycle,  $FwScalar_{x,y,m}$  (equation 5).

$$FwScalar_{x,y,m} = \frac{Fw_{x,y,m}}{FwMax_{x,y,m}} \text{ where } m = 1..12 \quad (4)$$

$$FwCor_{x,y,t} = FwMaxGLWD_{x,y} FwScalar_{x,y,t} \text{ where } t = 1..all \text{ months} \quad (5)$$

The adjusted SWAMPS-GLWD product results in a maximum wetland area of 10.5 Mkm<sup>2</sup>, and in agreement with the GLWD and other studies (Fluet-Chouinard *et al* 2014), but the product also maintains the seasonal cycle and inter-annual trends of inundation mapped by SWAMPS. Key wetland areas are retained in the SWAMPS-GLWD in areas such as Amazonia, the Congo Basin, and the Western Siberian Lowlands, which in previous studies have been poorly represented (Bohn *et al* 2015).

We also conducted a sensitivity test to account for how differences in view angle between the QSCAT and ASCAT instruments might influence trends in surface inundation. SWAMPS accounted for changes in the

angle-of-incidence between sensors by applying a time-averaged normalization approach to the backscatter retrievals (Schroeder *et al* 2015), however sensor-based offsets in grid cells with low surface inundation may affect the trends. We removed low surface-inundation grid cells (defined by their maximum annual value) using a per-pixel threshold of 0.5%, 1%, 2.5% and 5%, and compared the change in methane emissions for each scenario with no filter applied.

### Modeling protocol and other driver data

A common simulation protocol was followed by each of the wetland modeling teams (listed in table S1 available at [stacks.iop.org/ERL/12/094013/mmedia](https://stacks.iop.org/ERL/12/094013/mmedia)) using standardized climate, atmospheric CO<sub>2</sub> and dynamic wetland area data (used to map CH<sub>4</sub> producing regions), and also to specify boundary conditions for model spin-up and transient runs. CRU-NCEP v4.0 was used as the meteorology data, which includes long and shortwave radiation, air pressure, specific humidity, total precipitation, air temperature, and wind speed and direction. CRU-NCEP v4.0 combines the higher spatial resolution of CRU TS3.22 (Harris *et al* 2013) with the higher temporal resolution from the NCEP Reanalysis product (Kanamitsu *et al* 2002), to produce a meteorological forcing dataset that covers years 1901–2012 at 6 hourly temporal and 0.5 degree spatial resolution, and is used as the climate driver for biogeochemical models included in the annual Global Carbon Project CO<sub>2</sub> budget (Le Quéré *et al* 2015). Global atmospheric CO<sub>2</sub> concentrations were provided at an annual resolution for 1860–2012, with data prior to 1958 from ice cores (Joos and Spahni 2008) and after 1958 from the average of NOAA measurements at Mauna Loa (MLO) and the South Pole (SPO) stations.

Models were run to equilibrium during a spin-up phase where the first thirty years of climate data, 1901–1930, were recycled with pre-industrial CO<sub>2</sub> concentrations ~276 ppm). Soil texture data was prescribed using model-specific global soil databases such as the Harmonized World Soils Database (FAO/IIASA/ISRIC/ISSCAS/JRC 2012) and with pedo-transfer functions (i.e. Cosby *et al* 1984) to determine water-holding capacity. Land use (i.e. agriculture or pasture) and land-cover change were not simulated, and CH<sub>4</sub> emissions by fire excluded from our analysis. Modeling groups used their default vegetation distributions determined by either a dynamic vegetation model or by prescribed satellite vegetation products (Poulter *et al* 2015).

### Atmospheric CH<sub>4</sub> observations

Atmospheric observations of CH<sub>4</sub> were accessed from the NOAA ESRL cooperative air sampling network (Dlugokencky *et al* 1994). We carried out a comparison of wetland CH<sub>4</sub> emissions with atmospheric growth rate data from surface flask measurements at MLO and with the globally averaged marine surface annual mean dataset, which uses selected sites

**Table 1.** Wetland methane emissions in Tg CH<sub>4</sub> yr<sup>-1</sup> for each of the 12 TRANSCOM regions (Gurney *et al* 2003), with codes as defined in figure 1. The emissions are presented as averaged over the stabilization period (2000–2006), the increasing period (2007–2012) and for 2012. The uncertainty range is estimated as the standard deviation of the wetland CH<sub>4</sub> model ensemble ( $n = 11$ ).

Region	2000–2006	2007–2012	2012
<b>Boreal</b>			
Boreal N America (NABo)	25.1 ± 11.3	26.1 ± 11.8	27.1 ± 12.5
Boreal Eurasia (EuBo)	11 ± 5.3	11 ± 5.2	10.7 ± 5.2
Europe (EURO)	5.7 ± 2.5	5.9 ± 2.6	6.1 ± 2.6
<b>Temperate</b>			
N America (NATe)	16.2 ± 5.6	16.4 ± 5.7	17.6 ± 5.9
S America (SATE)	13.4 ± 3.6	12.1 ± 3.2	11.9 ± 3.4
Eurasia (EUTE)	15.1 ± 7.1	14.8 ± 7.2	14.9 ± 7.4
<b>Tropical</b>			
S America (TrSA)	38.5 ± 9.3	37.4 ± 9.2	36.8 ± 9.1
Asia (TrAs)	22.5 ± 3.7	23.2 ± 3.7	23.9 ± 3.8
Africa (TrAf)	8.4 ± 1.9	8.0 ± 1.7	8.3 ± 1.8
<b>Semi Arid</b>			
N Africa (NAfr)	8.5 ± 3.7	8.8 ± 3.6	8.3 ± 3.3
S Africa (SAfr)	9 ± 1.9	9.2 ± 2	9.2 ± 1.8
Australia (AUST)	2.7 ± 1.5	2.7 ± 1.4	2.6 ± 1.3
Global	184 ± 21.1	183.5 ± 23.1	185.7 ± 23.2

representative of a well-mixed marine boundary layer. In addition to anthropogenic contributions, the growth rate at MLO integrates terrestrial flux processes and has been demonstrated to be useful as a representative station for diagnosing CO<sub>2</sub> and CH<sub>4</sub> exchange between the biosphere and atmosphere (Fung *et al* 1991, Dlugokencky *et al* 1995, Bousquet *et al* 2006, Wang *et al* 2014, Meng *et al* 2015). Annual mean CH<sub>4</sub> concentrations from 2000–2012 were first detrended, removing the long-term increase in CH<sub>4</sub> concentrations following 2006, because we were interested in evaluating the role of interannual climate variability on CH<sub>4</sub> emissions (assuming minimal variability in OH at interannual timescales) and then using a conversion of 2.78 Tg CH<sub>4</sub> per ppb to estimate changes in the ‘atmospheric burden’ (Fung *et al* 1991). The interannual variability of CH<sub>4</sub> concentrations and emissions was then calculated as  $Y_i + Y_{(i+1)}$  (where  $Y = \text{year}$ ). As could be expected, the variability in the MLO observations was more highly correlated with wetland CH<sub>4</sub> emission variability than with the globally averaged observations, where the averaging across multiple, mainly marine, stations across latitudes partly dampens the contribution from land to inter-annual variability. Thus, in the following, only the MLO observations are used to discuss the contribution of the modeled fluxes to atmospheric variability.

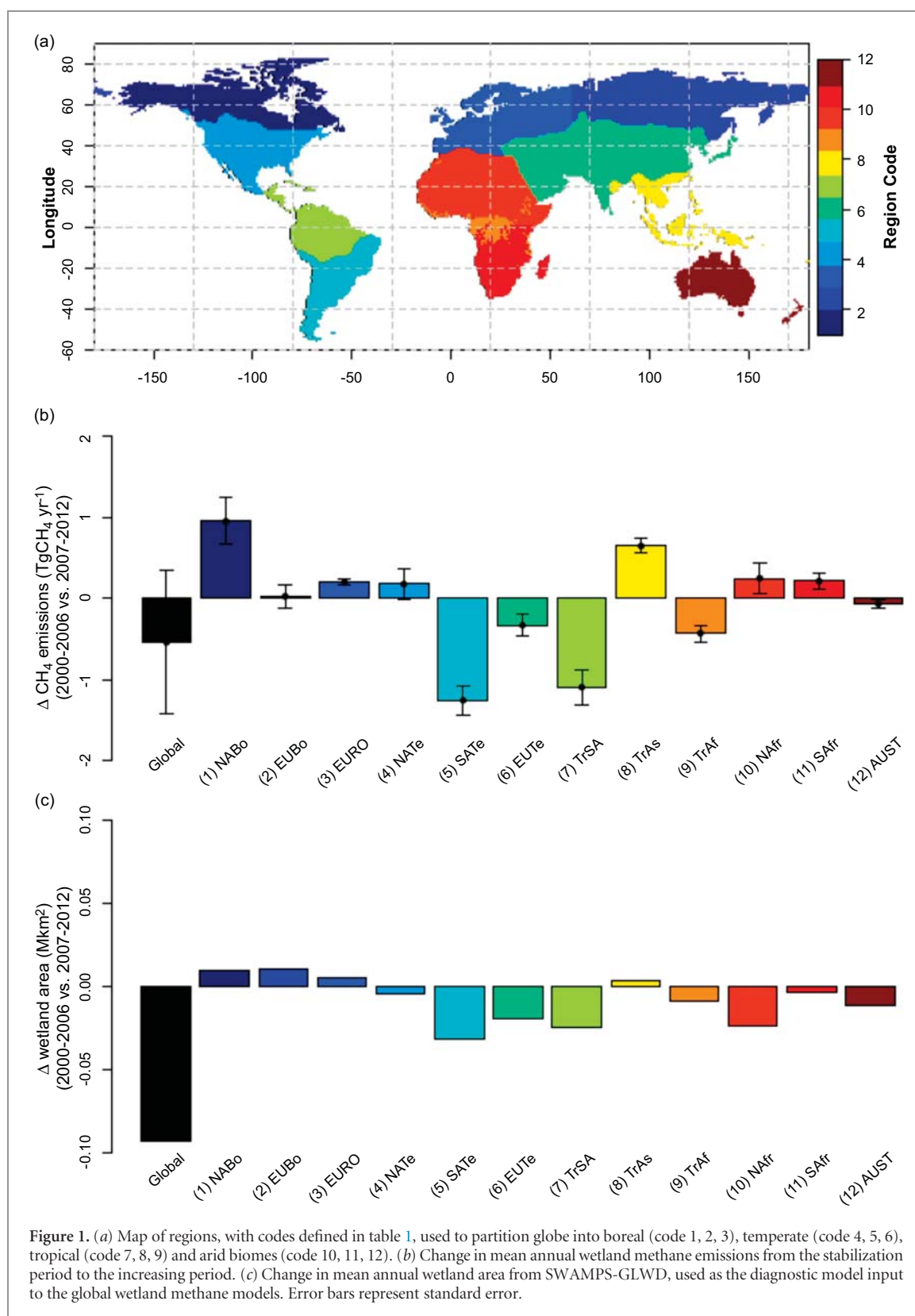
## Results

### Global and regional trends in wetland CH<sub>4</sub> emissions (2000–2012)

For the stabilization period (2000–2006), global wetland CH<sub>4</sub> emissions were estimated at  $184 \pm 21$  Tg CH<sub>4</sub> yr<sup>-1</sup>, where the uncertainty is estimated as one standard deviation of the model ensemble mean. Wetland emissions remained statistically similar during the period of renewed growth (2007–2012) at  $183 \pm 23$  Tg CH<sub>4</sub> yr<sup>-1</sup>, with a slightly larger value in the last year of analysis, 2012, of  $186 \pm 23$  Tg CH<sub>4</sub> yr<sup>-1</sup>

(table 1). For both time periods, tropical biomes, defined in figure 1(a) as regions 7 to 9, dominated the global flux with representative 2012 emissions, for example, of  $69 \pm 12$  Tg CH<sub>4</sub> yr<sup>-1</sup>, followed by boreal ( $44 \pm 19$  Tg CH<sub>4</sub> yr<sup>-1</sup>), temperate ( $44 \pm 10$  Tg CH<sub>4</sub> yr<sup>-1</sup>), and sub-tropical biomes ( $20 \pm 5$  Tg CH<sub>4</sub> yr<sup>-1</sup>). The global fluxes are consistent with a range of previously published estimates using satellite based approaches, i.e. 170 Tg CH<sub>4</sub> yr<sup>-1</sup> (Bloom *et al* 2010), atmospheric inversions, i.e. 149–159 Tg CH<sub>4</sub> yr<sup>-1</sup> (Ghosh *et al* 2015) and 165 ± 9 Tg CH<sub>4</sub> yr<sup>-1</sup> (Bousquet *et al* 2011), process-based models, i.e. 190 ± 39 Tg CH<sub>4</sub> yr<sup>-1</sup> (Melton *et al* 2013) and a combination of inversion and process-model, i.e. 172 Tg CH<sub>4</sub> yr<sup>-1</sup> (Spahni *et al* 2011).

Between the two time periods (the 2000–2006 ‘stabilization’ and the 2007–2012 ‘renewed growth’ periods), no statistically significant change in the average model ensemble emissions (two-sided Student’s  $t$ -test;  $\alpha = 0.1$ ) was found at the global scale or regionally (figure 2(a) and figure 3(a)). Among individual models, the change in global emissions between 2000–2006 and 2007–2012 ranged from a 5.4 Tg CH<sub>4</sub> yr<sup>-1</sup> decrease for ORCHIDEE to an increase of 4.8 Tg CH<sub>4</sub> yr<sup>-1</sup> for LPJ-MPI, with an ensemble average change of  $-0.5 \pm 0.9$  Tg CH<sub>4</sub> yr<sup>-1</sup> (figure 1(b)). At the regional scale (figure 1(b)), an increase in boreal wetland CH<sub>4</sub> emissions of  $1.2 \pm 0.3$  Tg CH<sub>4</sub> yr<sup>-1</sup> was found for the ensemble, with only CLM4.5 estimating reduced emissions of 0.2 Tg CH<sub>4</sub> yr<sup>-1</sup> and with LPJ-MPI providing the largest increase of 3.5 Tg CH<sub>4</sub> yr<sup>-1</sup>. Six of the individual models had statistically significant increasing trends for boreal CH<sub>4</sub> emissions (linear regression,  $p < 0.1$ ) and of these six, all models agreed with an increase in emissions occurring for June–August (JJA) and September–November (SON). A decrease in tropical emissions of  $0.9 \pm 0.3$  Tg CH<sub>4</sub> yr<sup>-1</sup> between 2000–2006 and 2007–2012 was observed across the model ensemble, with just two models estimating an increase



(CLM4.5 and LPJ-MPI, 0.1 and 1.1  $\text{Tg CH}_4 \text{ yr}^{-1}$ , respectively) and ORCHIDEE estimating the largest decrease of 3.1  $\text{Tg CH}_4 \text{ yr}^{-1}$ . Four of the individual models had a statistically significant ( $p < 0.1$ ) decrease in tropical  $\text{CH}_4$  emissions between JJA and SON. Changes in tropical wetland emissions were sensitive to the filtering of the low-surface inundated wetlands,

carried out to detect inter-sensor bias, but no statistically significant change was detected (table S3). A decrease in temperate regional emissions of  $1.4 \pm 0.4 \text{ Tg CH}_4 \text{ yr}^{-1}$  and almost no change in semi-arid emissions ( $0.4 \pm 0.2 \text{ Tg CH}_4 \text{ yr}^{-1}$ ) was also obtained for the ensemble, but with a larger spread across models than for the boreal and tropical regions.

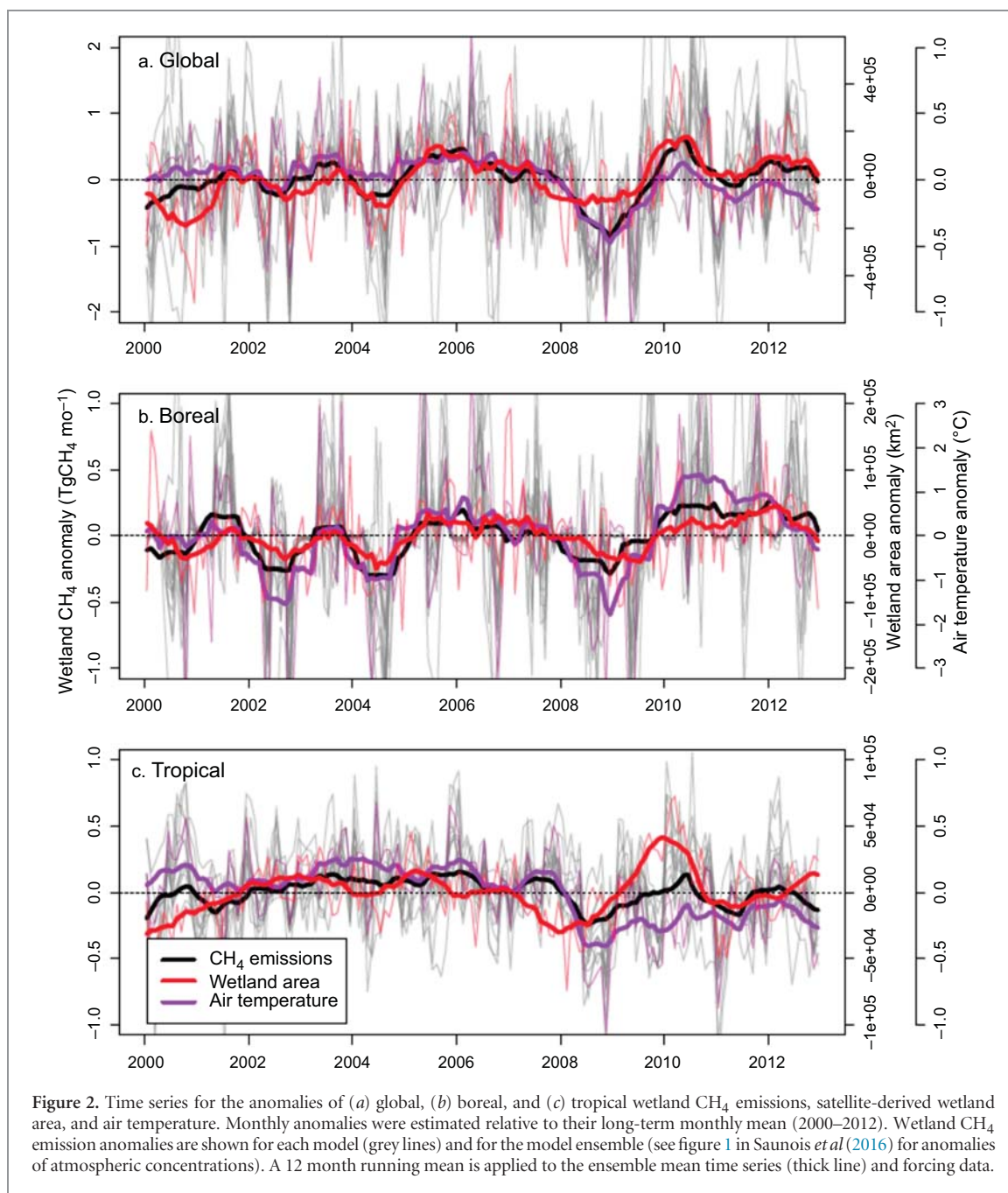


Figure 2. Time series for the anomalies of (a) global, (b) boreal, and (c) tropical wetland CH<sub>4</sub> emissions, satellite-derived wetland area, and air temperature. Monthly anomalies were estimated relative to their long-term monthly mean (2000–2012). Wetland CH<sub>4</sub> emission anomalies are shown for each model (grey lines) and for the model ensemble (see figure 1 in Saunio *et al* (2016) for anomalies of atmospheric concentrations). A 12 month running mean is applied to the ensemble mean time series (thick line) and forcing data.

### Climatic and physical drivers of regional CH<sub>4</sub> trends

During the 2000–2012 period, a linear regression analysis with climate forcing based on the Climate Research Unit, CRU TS3.22 (Harris *et al* 2013), masked to match wetland containing grid cells only (as an average over the 2000–2012 time period), revealed variable spatial and seasonal trends in precipitation and air temperature (for annual trends, see figure 3(c) and (d)). Total global December–February (DJF) precipitation increased by 2.5 mm yr<sup>-1</sup> ( $p < 0.05$ ) but did not change significantly in other seasons (figure 3(c)). Increasing boreal winter (DJF) precipitation contributed to about half of the annual global increase, 1.4 mm yr<sup>-1</sup> ( $p = 0.1$ ), with other boreal seasons showing no change, tropical DJF precipitation increased by 8.2 mm yr<sup>-1</sup> ( $p = 0.01$ ), and semi-arid DJF precipitation increased

by 1.8 mm yr<sup>-1</sup> ( $p = 0.04$ ). Global annual air temperature over wetlands was nearly constant (figure 3(d)), and increased at a rate of 0.02 °C yr<sup>-1</sup> in JJA ( $p < 0.05$ ) and 0.04 °C yr<sup>-1</sup> in SON ( $p < 0.05$ ). The change in global air temperature was mainly due to increasing air temperature in boreal regions with a significant ( $p < 0.1$ ) rate of increase of 0.06 °C yr<sup>-1</sup> from 2000–2012 in SON, and in tropical biomes where air temperature also increased slightly in JJA and SON at a rate of 0.02 °C yr<sup>-1</sup> ( $p < 0.1$ ). Cloud cover (not shown) increased by 0.1% yr<sup>-1</sup> ( $p = 0.05$ ) between March–May (MAM) in the tropics and decreased during boreal MAM by -0.2% yr<sup>-1</sup> ( $p = 0.03$ ).

Average annual maximum global wetland area for the merged SWAMPS-GLWD was 10.5 million km<sup>2</sup> (see Methods for comparison with original SWAMPS)



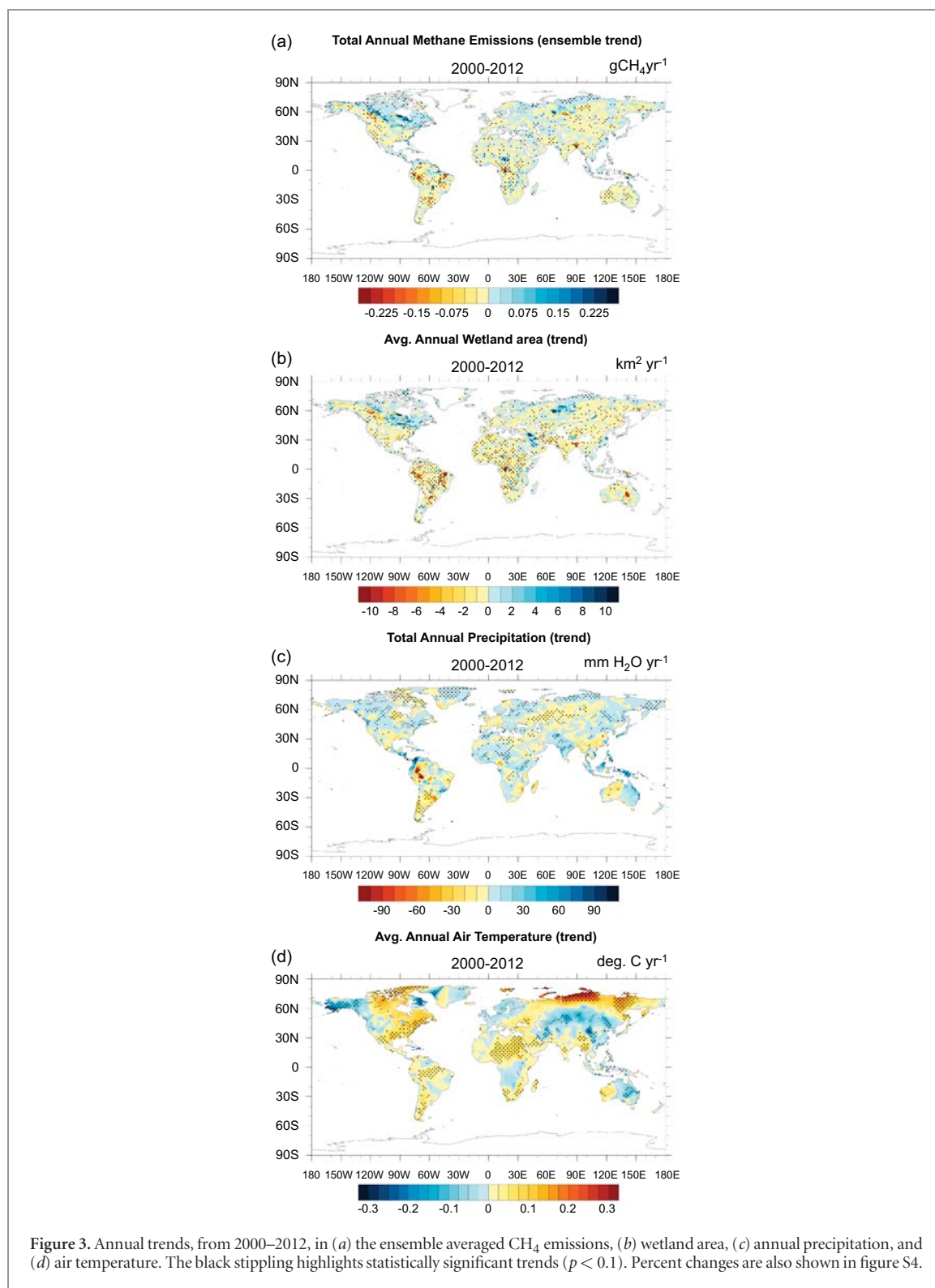


**Figure 3.** Annual trends, from 2000–2012, in (a) the ensemble averaged  $\text{CH}_4$  emissions, (b) wetland area, (c) annual precipitation, and (d) air temperature. The black stippling highlights statistically significant trends ( $p < 0.1$ ). Percent changes are also shown in figure S4.

and was in agreement with the GLWD inventoried global wetland area (Lehner and Doll 2004) used as the basis for several benchmarking activities (Fluet-Chouinard *et al* 2014, Bohn *et al* 2015). Globally and regionally, the SWAMPS-GLWD dataset had a similar seasonal phase (figure S1) for wetland area as GIEMS ( $R^2 > 0.85$  for all except the semi-arid region) yet SWAMPS-GLWD had larger seasonal amplitude because of the addition of permanent wetlands from

GLWD. The overlapping time period for GIEMS and SWAMPS, years 2000–2007, showed no significant trends globally or regionally for both datasets. Between the  $\text{CH}_4$  stabilization and renewed growth periods, global mean annual wetland area decreased by 93 000  $\text{km}^2$  (2% of average annual wetland area, figure 1(c) and figure 3(b)). At the seasonal scale, a large part of the decrease was explained by negative JJA trends in wetland area, where a statistically

significant decrease of  $27\,000\text{ km}^2\text{ yr}^{-1}$  was observed ( $p < 0.01$ ). Much of the seasonal decrease was explained by statistically significant changes in tropical, temperate, and semi-arid JJA wetland area of  $-4600$ ,  $-1400$ , and  $-6000\text{ km}^2\text{ yr}^{-1}$ , respectively, with additional changes in DJF tropical ( $-3500\text{ km}^2\text{ yr}^{-1}$ ) and semi-arid ( $-7300\text{ km}^2\text{ yr}^{-1}$ ) wetland area observed. In the boreal regions, wetland area increased by  $3000$  and  $16\,400\text{ km}^2\text{ yr}^{-1}$  in DJF and SON, respectively ( $p < 0.01$ ). Overall, a complex pattern of regional and seasonal contributions in declining global wetland area was observed, consistent with decadal and multi-decadal observations of land-water storage and open-water bodies (Dieng *et al* 2015, Donchyts *et al* 2016), and with tropical wetland area decreasing ( $-3.4\%$ ) and boreal wetland increasing ( $1.8\%$ ) in area (figures 2(b) and (c)) between the stabilization and the renewed growth periods.

### Sensitivity of CH<sub>4</sub> emissions to climate and wetland area

A partial correlation analysis was carried out to determine the effect of wetland area and climate on CH<sub>4</sub> emissions, and to determine the interaction between local climate and large-scale climatic teleconnections, including the Multivariate El Niño Index (MEI) and the North Atlantic Oscillation (NAO), on regional wetland area dynamics. Partial correlation analysis is an appropriate statistic to provide estimates on the correlation coefficient for a set of variables while simultaneously controlling for their interactions. The resulting partial correlations,  $r$ , range from  $-1$  to  $1$  with absolute values closer to unity reflecting higher explanatory power, either with a negative or positive relationship between the independent and dependent variables. Monthly time series for each variable were correlated for the period 2000–2012 and the data were not detrended beforehand because there were no significant trends detected.

The MEI and NAO represent two major global climatic teleconnections, with the MEI linking Pacific sea surface temperature anomalies (lagged by one month) with a warming and drying in tropical regions in its positive El Niño phase and a wetting of mid-latitude arid regions in its negative La Niña phase (Wolter and Timlin 1993). The MEI is similar in its temporal dynamics to the Oceanic Niño Index that uses sea surface temperature anomalies from the Niño 3.4 region. In contrast, the NAO measures the difference in air pressure between the Icelandic low and Azores high (Barnston and Livezey 1987), reflecting mid-to-high latitude climates, with a positive NAO characterized by above average annual temperature and wet winters in Eastern North America and northern Europe and below-average temperatures in the arctic. In contrast, during the negative NAO phase, cooler and drier than average conditions persist in eastern North America and northern Europe, with warmer than average conditions in the Arctic.

For the model ensemble, variability in global CH<sub>4</sub> emissions was most highly correlated with wetland area ( $r = 0.64$ ), followed by temperature ( $r = 0.37$ ) and with negligible correlations for precipitation ( $r = 0.09$ ) and cloud cover ( $r = 0.11$ ). A two to three month lag between the CH<sub>4</sub> emissions response and climate increased the precipitation correlation by a small amount, from  $0.09$  (with no time lag) to  $0.11$  with a one month lag. Monthly to seasonal scale lags have also been observed in atmospheric inversion and hydrologic studies (Papa *et al* 2015, Ribeiro *et al* 2016, Wilson *et al* 2016) where transit time of water within a basin and other hydrologic processes, such as evapotranspiration, decouple the more immediate interactions between precipitation and emissions. At the regional scale, wetland area was also the most important variable for CH<sub>4</sub> emissions, with a correlation of  $0.89$  and  $0.72$  in tropical and temperate regions, respectively. In contrast, for the individual models, global CH<sub>4</sub> emission for JULES and LPJ-MPI was more highly correlated with air temperature than with wetland area due to their greater temperature sensitivity than other models, whereas the remaining models were correlated first with wetland area, and then with air temperature followed by smaller precipitation or cloud cover correlations. The ranking of global wetland area as the main driver of CH<sub>4</sub> production, followed by temperature and then precipitation was similar for the boreal, tropical, temperate, and arid regions, and consistent with results from a multi-model CH<sub>4</sub> sensitivity experiment carried out by Melton *et al* (2013). Overall, the higher air temperature sensitivity of CH<sub>4</sub> emissions was responsible for moderate correlations, with varying time lags ( $t$  minus number months,  $n$ ), with the MEI for boreal ( $r_{t-0} = -0.16$ ), tropical ( $r_{t-6} = 0.33$ ), and temperate emissions ( $r_{t-3} = 0.24$ ), with the NAO also only weakly correlated with the model ensemble for boreal regions ( $r_{t-3} = -0.13$ ). At the global scale, the MEI and NAO were most highly correlated with CH<sub>4</sub> emissions with a five-month lag,  $r_{t-5} = 0.26$  and  $r_{t-5} = 0.08$ , respectively, slightly lower than in previously published studies (Bousquet *et al* 2006, Hodson *et al* 2011).

Wetland area dynamics from the SWAMPS-GLWD dataset at global and regional scales were moderately correlated with air temperature (masked for wetland grid cells),  $r_{t-0} = 0.24$  globally, and  $r_{t-0} = 0.33$  for boreal regions, suggesting surface-flooding increased following seasonal permafrost thaw under warmer temperatures (Schuur *et al* 2015). Precipitation (also masked for wetland grid cells) was weakly correlated with global wetland area ( $r_{t-0} = -0.11$ ), and with wetland area in temperate ( $r_{t-0} = 0.18$ ), tropical ( $r_{t-0} = -0.12$ ), and arid regions ( $r_{t-0} = -0.15$ ). The introduction of time lags (up to +6 months) in the climate variables did not significantly improve the correlations with wetland area except in semi-arid regions where a one month lag increased the precipitation correlation with wetland area ( $r_{t-1} = 0.30$ ). These results highlight the importance of incorporating sub-grid cell

topographic variation, as well as cell-to-cell interactions, when modeling feedbacks between hydrologic flow paths and surface inundation dynamics. At the global scale, the MEI was positively, albeit weakly, correlated with wetland area ( $r_{t-5} = 0.33$ ) mainly because of the relationship with tropical ( $r_{t-5} = 0.29$ ) and temperate wetland dynamics ( $r_{t-5} = 0.25$ ). Boreal regions were negatively correlated with MEI with a one-month lag ( $r_{t-1} = -0.14$ ) and both the MEI and NAO positively correlated with wetland area in temperate regions ( $r_{t-0} = 0.27$  and  $r_{t-0} = 0.15$ , respectively). The moderate correlations, compared with earlier studies, were partly due to the short time series, where between 2000–2012, the NAO was mainly in negative phase (meaning below-average precipitation in mid-high latitudes, cooler eastern North America and northern European temperatures, and warmer arctic conditions), and no large El Niño events, whereas a record magnitude La Niña lasted from late 2009 to 2011 (Evans and Boyer-Souchet 2012). In addition, our regional definitions may also interfere with the strength of the teleconnection correlations by introducing a mix of biome types with varying climatic responses (Zhang *et al* 2015).

## Discussion

### High latitude increases and low latitude decreases in CH<sub>4</sub> emissions

From 2000–2012, global wetland emissions appear to have remained stable and with regional increasing and decreasing trends closely compensating for one another, with no net contribution to the observed renewed atmospheric growth rate. By shifting the period of comparison to 2003–2005 and 2010–2012 to evaluate the sensitivity of our definition for the stabilization and renewed growth periods, we find only a slightly larger increase in emissions, from  $185 \pm 22$  Tg CH<sub>4</sub> yr<sup>-1</sup> to  $186 \pm 24$  Tg CH<sub>4</sub> yr<sup>-1</sup>, an average  $1.23 \pm 1.1$  Tg CH<sub>4</sub> increase and also not large enough to explain the 2007 renewed atmospheric CH<sub>4</sub> growth rate of  $\sim 17$  Tg CH<sub>4</sub> yr<sup>-1</sup>. Additionally, the increase between the 2003–2005 and 2010–2012 periods is not robust and almost entirely driven by just one model, which also has the highest temperature sensitivity, LPJ-MPI ( $12.6$  Tg CH<sub>4</sub> yr<sup>-1</sup> increase). The increase in boreal emissions from 2000–2012 appears to be closely linked to both increasing air temperature and wetland area, with an anomalously warm event in 2007 (Bruhwiler *et al* 2014). In high latitude regions, evidence for warming air temperature is well documented and the feedbacks between increasing air temperature, sea-ice cover loss, and terrestrial CH<sub>4</sub> emissions is becoming increasingly clear (Karl *et al* 2015, Parmentier *et al* 2015). Finer-temporal and spatial remote-sensing based analyses are also consistent with the evidence presented here for a net increase in boreal wetland area and CH<sub>4</sub> emissions from 2003 to 2011 (Watts *et al* 2014). Overall, these changes are

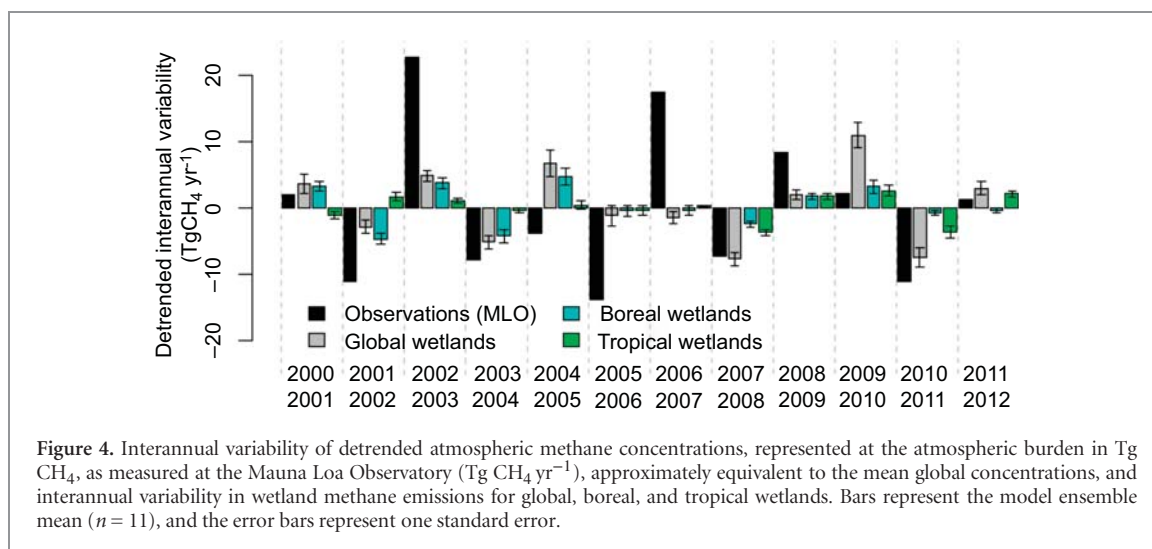
consistent with field observations (Sweeney *et al* 2016) and with what could be expected from projected climate change and warming impacts on high latitude systems that link temperature sensitivity as a dominant control on arctic wetland CH<sub>4</sub> emissions (Schaefer *et al* 2011, Chen *et al* 2015, Schuur *et al* 2015).

In tropical regions, high interannual variability in precipitation makes detecting decadal scale carbon-cycle trends challenging (Jung *et al* 2010, Zhang *et al* 2015). In terms of wetland area dynamics, Papa *et al* (2010) reported a decrease of  $19\,600$  km<sup>2</sup> yr<sup>-1</sup> in tropical surface inundation between 1993 and 2005 based on the GIEMS data, and losses of tropical surface inundation appear to have continued through 2012 at a rate of  $4000$  km<sup>2</sup> yr<sup>-1</sup> (Schroeder *et al* 2015). As a consequence, declining tropical wetland CH<sub>4</sub> emissions have been found in a range of studies using GIEMS, for example, Meng *et al* (2015), who found a decline of  $1.68$  Tg CH<sub>4</sub> yr<sup>-1</sup> from 1993–2004. However, even with models that used fixed or static, i.e. the GLWD, rather than dynamic areal extent of wetlands, declining tropical wetland CH<sub>4</sub> emissions were simulated (Zhu *et al* 2015), suggesting that trends in climatic drivers that force changes in wetland area may be an equally important constraint on tropical CH<sub>4</sub> production. Over Amazonia and the Congo Basins, large consecutive droughts, in 2005 and 2010, combined with regional warming, have resulted in widespread declines in tropical forest canopy greenness (Hilker *et al* 2014, Zhou *et al* 2014). These Amazonian droughts are superimposed on an intensification of the hydrologic cycle in the wet season (Gloor *et al* 2013) rather than an increase in the duration of the wet season throughout the year. Declining precipitation trends between 2010–2012 were observed in Western Amazonia and Eastern Congo, but over Southeast Asia, increases in precipitation were observed (figure 3(c)). Degradation of global wetlands due to human activities is also a large component in declining wetland function (Petrescu *et al* 2015, Donchyts *et al* 2016), and losses of tropical wetland area due to drainage are the highest globally, ranging up to 2% per year (Davidson 2014, Papa *et al* 2015).

Outside of tropical regions, declining wetland area in temperate regions also coincided with long-term drying of soils from 1950–2005 (Mueller and Zhang 2015), however the precipitation trends from 2000–2012 of relevance in this study suggest soil moisture actually increased in this time period (figure 3(c)). Semi-arid regions, i.e. eastern Australia and South America, showed decreasing annual precipitation trends, despite large swings in seasonal precipitation related to a series of strong La Niña events (Boening *et al* 2012).

### Role of teleconnections on interannual variability of wetland area and CH<sub>4</sub> emissions

ENSO has previously been highlighted as a key driver of interannual variability in global wetland CH<sub>4</sub> production (Bousquet *et al* 2006, Hodson *et al* 2011,



Dalsøren *et al* 2015). Here, we find a possibly lower role for ENSO in driving global wetland CH<sub>4</sub> production that is due in part to i) the duration of the brief time series where no strong El Niño was observed and ii) the use of a new integrated wetland–surface–water dataset. Previous analyses have used longer time series, such as Hodson *et al* (2011), who scaled modeled soil-moisture to wetland area based on a GIEMS calibrated hydrologic model. For the time period 1950–2005 they found a slightly higher global correlation of global CH<sub>4</sub> emissions with ENSO,  $R^2 = 0.39$  (with a three-month lag) and  $R^2 = 0.56$  for the tropics. In addition, using an atmospheric inversion, Bousquet *et al* (2006) partitioned CH<sub>4</sub> emissions to anthropogenic and natural sources for the period 1984–2003. The study concluded that the dominant role of CH<sub>4</sub> surface sources was from high interannual variability of wetland area that was synchronized with ENSO. The longer 1950–2005 time period includes a wider range of both positive and negative phase ENSO events, whereas the 2000–2012 period evaluated here includes two major La Niña and only moderate El Niño events.

In addition, many studies have relied on GIEMS surface inundation data to constrain wetland areal dynamics, and have found GIEMS to be highly correlated with ENSO (Prigent *et al* 2007). While the new SWAMPS-GLWD dataset used here was found to enhance seasonal variation in wetland area, the dataset also partially decoupled the interannual surface-water variability from climate because of the integration of permanently inundated wetlands (with no surface flooding) from GLWD, to address known limitations in microwave remote sensing of wetlands, particularly in forested areas (Bohn *et al* 2015). We evaluated how the development of the SWAMPS-GLWD wetland dynamics dataset affected interannual variability (IAV) of wetland CH<sub>4</sub> emissions by comparing with the detrended observations of atmospheric CH<sub>4</sub> variability from MLO. We found the observed IAV at MLO to range from  $-13$  to  $22$  Tg CH<sub>4</sub> yr<sup>-1</sup> from 2000 to 2012 (figure 4). In comparison, the IAV of

the SWAMPS-GLWD driven wetland model ensemble ranged from  $-13$  to  $19$  Tg CH<sub>4</sub> yr<sup>-1</sup>, and across models, the range varied from small IAV ( $-8$  to  $1$  Tg CH<sub>4</sub> yr<sup>-1</sup> for CTEM) to large IAV ( $3$  to  $19$  Tg CH<sub>4</sub> yr<sup>-1</sup> for ORCHIDEE). Compared to observations, the sensitivity of the model ensemble results provide confidence in the use of SWAMPS-GLWD for partially driving a CH<sub>4</sub> IAV consistent with previous top-down and isotopic studies, e.g. Bousquet *et al* (2006), that demonstrate wetland CH<sub>4</sub> emissions explain a large portion of the IAV in atmospheric growth ( $r = 0.46$  for the model ensemble, with the individual models ranging from  $r = 0.2$  (TRIPLEX-GHG) to  $r = 0.6$  (SDGVM)). Notably, the contribution of boreal wetlands to global CH<sub>4</sub> IAV appears to decline from 2000–2012 relative to an increase from tropical contributions (figure 4), however, overall we found a trend toward decreasing IAV in the observed CH<sub>4</sub> growth rate. Wildfires, not considered in this study, can contribute between  $10$ – $20$  Tg CH<sub>4</sub> yr<sup>-1</sup> of emission IAV, however no significant trend over time has been observed to date (van der Werf *et al* 2006, van der Werf *et al* 2010, Worden *et al* 2013). Additionally, year-to-year variability in the atmospheric oxidative sink for methane may also affect variability in growth rate anomalies (Rigby *et al* 2008).

#### Uncertainties from additional biogenic CH<sub>4</sub> sources

The depletion of atmospheric  $\delta^{13}\text{C}$  of CH<sub>4</sub> since 2007 presents three scenarios, (i) a change in average biogenic wetland  $\delta^{13}\text{C}$  source signature, (ii) an overall increasing biogenic source, (iii) a decreasing thermogenic or pyrogenic source, or some combination of all (Kirschke *et al* 2013). Thermogenic, or fossil-fuel related emissions, are unlikely to have decreased in recent years (Bergamaschi *et al* 2013, Nisbet *et al* 2014), and recent studies based on isotopic  $\delta^{13}\text{C}$  confirm a large biogenic source (Dlugokencky *et al* 2011, Rice *et al* 2016, Schaefer *et al* 2016). In addition to the wetland types considered in this study, there are several additional sources of biogenic emissions that

could contribute to the depletion of atmospheric  $\delta^{13}\text{C}$ . These include river systems (Bastviken *et al* 2011, Borges *et al* 2015), lakes (Verpoorter *et al* 2014, Tan and Zhuang 2015), and agriculture (Leff *et al* 2004, Chen *et al* 2013). For example, taken together, river and lake system  $\text{CH}_4$  emissions are highly uncertain and are estimated to emit as much as  $100 \pm 50$  Tg  $\text{CH}_4 \text{ yr}^{-1}$  (Bastviken *et al* 2011), or the equivalent of  $\sim 30\%$ – $50\%$  of global wetland emissions, and would require a reassessment of other source terms to close the global methane budget (Saunio *et al* 2016). These emission hotspots are also geographically distributed across arctic (Walter Anthony *et al* 2014), temperate (Chen *et al* 2013) and tropical systems (Borges *et al* 2015). The temporal response of agricultural  $\text{CH}_4$  emissions (excluding biomass burning) is poorly understood, yet agriculture accounts for about 30% of total wetland  $\text{CH}_4$  emissions (Kirschke *et al* 2013) and is produced from rice cultivation and enteric fermentation of livestock ruminants. These agricultural emissions can change on annual to decadal time scales in response to climate (Li *et al* 2002), but also in response to farming practices where land management can rapidly respond to socio-economic drivers (Chen *et al* 2013) and contribute to atmospheric IAV and to long-term trends (Tian *et al* 2016).

### Reducing biogenic source uncertainty

By using a multi-model approach to investigate the temporal trends and spatial patterns in global  $\text{CH}_4$  emissions, the model uncertainty can be quantified more robustly. Here, the sources of uncertainty can be partitioned to (i) driver data, (ii) model structure, and (iii) parameter uncertainty. By providing a consistent set of climate, atmospheric  $\text{CO}_2$ , and wetland area data, the model spread was reduced from 123 Tg  $\text{CH}_4 \text{ yr}^{-1}$  (WETCHIMP, which used a similar model ensemble) to 80 Tg  $\text{CH}_4 \text{ yr}^{-1}$  (this study). This reduction highlights that uncertainties in wetland area are almost equally important to our mechanistic understanding of *in situ*  $\text{CH}_4$  production and consumption processes. Combining SWAMPS and GLWD led to wetland area estimates consistent with more detailed regional estimates for Amazonia (Wilson *et al* 2007, Draper *et al* 2014, Hess *et al* 2015), southeast Asia (Hooijer *et al* 2010), and high-latitude systems, such as the Western Siberia Lowlands (Bohn *et al* 2015, Zhang *et al* 2016b).

Model structure is another key source of uncertainty (Wania *et al* 2013, Xu *et al* 2016a), as illustrated by the range of temperature-emission sensitivities for the current model ensemble. About half of the models used here (JULES, LPJ-wsl, ORCHIDEE, SDGVM, CTEM) were based on the semi-empirical model approach of Christensen *et al* (1996), whereas the other models (LPX-Bern, LPJ-MPI, CLM4.5, TRIPLEX-GHG) were based on more mechanistic first order approaches based

on the framework developed by Walter *et al* (2001), see table S2 for a summary. One topic of large uncertainty are the oxidative processes that consume  $\text{CH}_4$  (Ridgwell *et al* 1999), and that may change over time and alter the  $\text{CO}_2$ : $\text{CH}_4$  production ratios used in the semi-empirical approaches (Curry 2007). However, there was no clustering of model structure in terms of global or regional emission trends.

In addition to meteorological and wetland area interannual variability, atmospheric  $\text{CO}_2$  rose by 24 ppm to 393 ppm from 2000 to 2012 (based on observations from Mauna Loa, MLO). Net primary production in carbon cycle models tends to respond positively to trends in elevated  $\text{CO}_2$  (Hickler *et al* 2008), and would be expected to provide a sustained increase in substrate in the form of soil organic carbon for anaerobic processes to produce  $\text{CH}_4$ . A strong  $\text{CO}_2$  driven response in  $\text{CH}_4$  emissions was not observed by the ensemble mean because of the high IAV of climate and wetland area that appear to be more limiting for  $\text{CH}_4$  emissions than substrate. Over longer timescales, i.e. multi-decadal to centennial, a strong  $\text{CO}_2$  feedback on  $\text{CH}_4$  emissions is expected, with simulated increases in global emissions of up to  $73\% \pm 49\%$  at 857 ppm  $\text{CO}_2$  (Melton *et al* 2013).

Lastly, model parameters are difficult to robustly estimate because  $\text{CH}_4$  production occurs in complex landscapes where anaerobic soil conditions can be very heterogeneous. To estimate emissions at scales of 50  $\text{km}^2$  or larger, where  $\text{CH}_4$  production may be occurring in small topographic depressions, remains a large challenge (Lara *et al* 2015, Shi *et al* 2015). While the area-weighted monthly-average flux estimates for the model ensemble ranged within observations, i.e. from 2.7 to 3.9  $\text{g CH}_4 \text{ m}^{-2} \text{ month}^{-1}$  globally, 0.7 to 3.1  $\text{g CH}_4 \text{ m}^{-2} \text{ month}^{-1}$  for boreal wetlands (observations 2–4  $\text{g CH}_4 \text{ m}^{-2} \text{ month}^{-1}$  in boreal systems (Turetsky *et al* 2014), and 5.2 to 8.2  $\text{g CH}_4 \text{ m}^{-2} \text{ month}^{-1}$  for tropical wetlands (observations 0.1 to 29  $\text{g CH}_4 \text{ m}^{-2} \text{ month}^{-1}$  (Sjogersten *et al* 2014). Benchmarking of process models with flux tower measurements or airborne campaigns remains critical for improving model structure and parameters (Miller *et al* 2016) and addressing scaling artifacts that may obscure non-linear methane production and consumption processes.

## Conclusions

### Key findings

Interpreting the interannual and decadal dynamics of the  $\text{CH}_4$  atmospheric growth rate has presented significant challenges over the past three decades, with the sources and sinks remaining poorly understood (Kirschke *et al* 2013). Using an ensemble of global wetland models constrained with satellite and inventory based surface inundation and wetland area seasonality and trends, we now provide a comprehensive and updated estimate of the role of wetlands in the recent

increase of the atmospheric growth rate that began in 2007. We show that the role of wetlands in the renewed period of atmospheric CH<sub>4</sub> growth appears minimal to non-existent, and that:

- At the global scale, wetland CH<sub>4</sub> emissions have remained constant from 2000–2012 at  $184 \pm 22$  Tg CH<sub>4</sub> yr<sup>-1</sup> but that significant spatial variability in trends are masked by the global perspective (figure S2 and S3).
- In boreal regions, increasing CH<sub>4</sub> emissions corresponds to increasing wetland area and air temperature, whereas in the tropics, decreasing wetland area and large variability in precipitation has led to decreased emissions.
- At global and the regional scales defined in our study, the role of climatic teleconnections such as ENSO and the NAO are smaller than what has been reported in previous work; however, we confirm that the IAV of the atmospheric growth rate is largely explained by wetlands.
- The interannual variability in global wetland emissions is dominated by boreal regions from 2000–2006 and then with increasing contribution from tropical regions possibly coinciding with larger droughts over Amazonia and the Congo Basin (figure 4). However, there has been no consistent shift in the IAV of wetland CH<sub>4</sub> emissions over the 2000–2012 time period (figure 4).
- The range of the modelled interannual variability in global wetland emissions in 2007–2012 is similar to the IAV observed at the MLO station, while it is less than observed for 2000–2006. Therefore, the period 2000–2006 is anomalous not only due to the absent trend in the growth rate of atmospheric CH<sub>4</sub> concentrations, but also due to anomalously high IAV not fully explained by natural wetland emissions.
- Our results, interpreted in the context of a depletion in atmospheric  $\delta^{13}\text{C}$  observed since 2007, suggests that either a shift in  $\delta^{13}\text{C}$  biogenic source signature occurred or other agricultural biogenic sources are required to explain the recent and sustained atmospheric increase in CH<sub>4</sub>, or that, less likely, a decrease in thermogenic and pyrogenic emission has occurred. This is consistent with recent work of Schaefer *et al* (2016) who present isotopic evidence suggesting an increasing role of livestock and agriculture in the growth rate of atmospheric CH<sub>4</sub>.
- The pattern of increasing high-latitude emissions and possibly decreasing to stable tropical emissions are consistent with climate change projections that forecast a general increase in boreal air temperatures and a decrease in tropical precipitation (Scholze *et al* 2006). Thus the past decade presents an observational test case for climate and socio economic impact studies on CH<sub>4</sub> production (Lawrence *et al* 2015, Petrescu *et al* 2015).
- To reduce uncertainties in wetland dynamics mapping we recommend that (1) multi-platform remote sensing using both radar and optical observations are integrated at higher spatial resolution to resolve issues associated with low-detection probabilities in closed-forest canopy regions, (2) that inter-sensor calibration and effects on inter-annual and seasonal trends are clearly accounted for, and (3) that ground-based wetland inventories are continually updated and made available to benchmark and calibrate remote sensing algorithms, and with clear terminology to avoid double counting.

## Acknowledgments

We acknowledge the data providers, especially for updating the gridded climate (CRU) and CO<sub>2</sub> and CH<sub>4</sub> concentration time series (NOAA ESRL). B.P., P.C., P.B. were supported by the EU FP7 GEOCARBON Programme (283080) and B.P. and Z.Z. were supported on the Swiss CCES MAIOLICA2 project #42V01 and F.J. and R.S. acknowledge support by the Swiss National Science Foundation and the EU FP7 project Past4Future (grant no. 243908). Met Office authors were supported by the Joint UK DECC/Defra Met Office Hadley Centre Climate Programme (GA01101). W.R., C.K., and X.X. were supported by the Director, Office of Science, Office of Biological and Environmental Research of the US Department of Energy under Contract No. DE-AC2-5CH11231. H.T. and B.Z. were supported by NASA grants (NNX14AF93G; NNX14AO73G) and NSF grants (AGS 1243232, CNH1210360). D.B, D.W, and L.T gratefully acknowledge support by NERC grant (R/131682). J.G.C. thanks the support from the National Environmental Science Program—Earth System and Climate Change Hub. J.G.C. thanks the support from the National Environmental Science Program—Earth System and Climate Change Hub. S.F.A., A.I. and M.S. were supported by the Environment Research and Technology Development Fund (2-1710) of the Ministry of the Environment, Japan, and Environmental Restoration and Conservation Agency. T.K. was supported by the German Ministry of Education and Research (grants no. 03G0836C and 01LP1507B).

## ORCID iDS

Victor Brovkin  <https://orcid.org/0000-0001-6420-3198>

Nicola Gedney  <https://orcid.org/0000-0002-2165-5239>

Zhen Zhang  <https://orcid.org/0000-0003-0899-1139>

Josep Canadell  <https://orcid.org/0000-0002-8788-3218>

Benjamin Poulter  <https://orcid.org/0000-0002-9493-8600>

## References

- Adam L, Doll P, Prigent C and Papa F 2010 Global-scale analysis of satellite-derived time series of naturally inundated areas as a basis for floodplain modeling *Adv. Geosci.* **27** 45–50
- Aydin M, Verhulst K R, Saltzman E S, Battle M O, Montzka S A, Blake D R, Tang Q and Prather M J 2011 Recent decreases in fossil-fuel emissions of ethane and methane derived from firm air *Nature* **476** 198–201
- Barnston A G and Livezey R E 1987 Classification, seasonality and persistence of low-frequency atmospheric circulation patterns *Mon. Weather Rev.* **115** 1083–126
- Bastviken D, Tranvik L J, Downing J A, Crill P M and Enrich-Prast A 2011 Freshwater methane emissions offset the continental carbon sink *Science* **331** 50
- Bergamaschi P *et al* 2013 Atmospheric CH<sub>4</sub> in the first decade of the 21st century: inverse modeling analysis using SCIAMACHY satellite retrievals and NOAA surface measurements *J. Geophys. Res.* **118** 7350–69
- Bloom A A, Palmer P I, Fraser A, Reay D S and Frankenberg C 2010 Large-Scale controls of methanogenesis inferred from methane and gravity spaceborne data *Science* **327** 322–5
- Boening C, Willis J K, Landerer F W, Nerem R S and Fasullo J 2012 The 2011 La Niña: so strong, the oceans fell *Geophys. Res. Lett.* **39** L19602
- Bohn T J *et al* 2015 WETCHIMP-WSL: intercomparison of wetland methane emissions models over West Siberia *Biogeosciences* **12** 3321–49
- Borges A *et al* 2015 Globally significant greenhouse-gas emissions from African inland waters *Nat. Geosci.* **8** 637–42
- Bousquet P *et al* 2006 Contribution of anthropogenic and natural sources to atmospheric methane variability *Nature* **443** 439–43
- Bousquet P *et al* 2011 Source attribution of the changes in atmospheric methane for 2006–2008 *Atmos. Chem. Phys.* **11** 3689–700
- Bruhwliler L, Dlugokencky E, Masarie K, Ishizawa M, Andrews A, Miller J, Sweeney C, Tans P and Worthy D 2014 CarbonTracker-CH<sub>4</sub>: an assimilation system for estimating emissions of atmospheric methane *Atmos. Chem. Phys.* **14** 8269–93
- Cao M, Marshall S and Gregson K 1996 Global carbon exchange and methane emissions from natural wetlands: application of a process based model *J. Geophys. Res.* **101** 14399–414
- Chen H, Zhu Q, Peng C, Wu N, Wang Y, Fang X, Jiang H, Xiang W, Chang J, Deng X and Yu G 2013 Methane emissions from rice paddies natural wetlands, and lakes in China: synthesis and new estimate *Glob. Change Biol.* **19** 19–32
- Chen X, Bohn T J and Lettenmaier D P 2015 Model estimates of climate controls on pan-arctic wetland methane emissions *Biogeosci. Discuss.* **12** 5941–89
- Christensen T R, Prentice I C, Kaplan J O, Haxeltine A and Sitch S 1996 Methane flux from northern wetlands and tundra: an ecosystem source modelling approach *Tellus* **48B** 652–61
- Ciais P *et al* 2013 Carbon and other biogeochemical cycles *Climate Change 2013: The Physical Science Basis. Contribution of Working Group I to the Fifth Assessment Report of the Intergovernmental Panel on Climate Change* ed T F Stocker, D Qin, G K Plattner, M Tignor, S K Allen, J Boschung, A Nauels, Y Xia, V Bex and Midgley P M (Cambridge: Cambridge University Press) ch 6
- Cosby B J, Hornberger G M, Clapp R B and Ginn T R 1984 A statistical exploration of the relationships of soil moisture characteristics to the physical properties of soils *Water Resour. Res.* **20** 682–90
- Curry C L 2007 Modeling the soil consumption of atmospheric methane at the global scale *Glob. Biogeochem. Cycles* **21** GB4012
- Dalsøren S B, Myhre C L, Myhre G, Gomez-Pelaez A J, Søvde O A, Isaksen I S A, Weiss R F and Harth C M 2015 Atmospheric methane evolution the last 40 years *Atmos. Chem. Phys. Discuss.* **2015** 30895–957
- Davidson N C 2014 How much wetland has the world lost? Long-term and recent trends in global wetland area *Mar. Freshw. Res.* **65** 934–41
- Dieng H B, Champollion N, Cazenave A, Wada Y, Schrama E and Meysignac B 2015 2012 land water storage change over 2003–2013 estimated from a global mass budget approach *Environ. Res. Lett.* **10** 124010
- Dlugokencky E J *et al* 2009 Observational constraints on recent increases in the atmospheric CH<sub>4</sub> burden *Geophys. Res. Lett.* **36** L18803
- Dlugokencky E J, Crotwell A M, Lang P M and Masarie K A 2015 Atmospheric methane dry air mole fractions from quasi-continuous measurements at Barrow, Alaska and Mauna Loa, Hawaii, 1986–2014, Version: 2015-04-28 (<ftp.cmdl.noaa.gov/ccg/ch4/in-situ/>)
- Dlugokencky E J, Masarie K A, Lang P M and Tans P P 1999 Continuing decline in the growth rate of the atmospheric methane burden *Nature* **393** 447–50
- Dlugokencky E J, Nisbet E G, Fisher R and Lowry D 2011 Global atmospheric methane: budget, changes and dangers *Phil. Trans. R. Soc. Lond. A* **369** 2058–72
- Dlugokencky E J, Steele L P, Lang P M and Masarie K 1994 The growth rate and distribution of atmospheric methane *J. Geophys. Res.* **99** 17021–43
- Dlugokencky E J, Steele L P, Lang P M and Masarie K 1995 Atmospheric methane at Mauna Loa and Barrow observatories: presentation and analysis of *in situ* measurements *J. Geophys. Res.* **100** 103–23
- Donchyts G, Baart F, Winsemius H, Gorelick N, Kwadijk J and van de Giesen N 2016 Earth's surface water change over the past 30 years *Nat. Clim. Change* **6** 810–13
- Draper F C, Roucoux K H, Lawson I T, Mitchard E T A, Honorio Coronado E N, Lahteenoja O, Torres Montenegro L, Valderrama E, Zarate R and Baker T R 2014 The distribution and amount of carbon in the largest peatland complex in Amazonia *Environ. Res. Lett.* **9** 124017
- Evans J P and Boyer-Souchet I 2012 Local sea surface temperatures add to extreme precipitation in northeast Australia during La Niña *Geophys. Res. Lett.* **39** L10803
- FAO/IIASA/ISRIC/ISSCAS/JRC 2012 *Harmonized World Soil Database* (version 1.21) (FAO and IIASA: Italy and Laxenburg)
- Fluet-Chouinard E, Lehner B, Rebelo L-M, Papa F and Hamilton S K 2014 Development of a global inundation map at high spatial resolution from topographic downscaling of coarse-scale remote sensing data *Remote Sens. Environ.* **158** 348–61
- Friedl M A, Sulla-Menashe D, Tan B, Schneider A, Ramankutty N, Sibley A and Huang X 2010 MODIS collection 5 global land cover: algorithm refinements and characterization of new datasets *Remote Sens. Environ.* **114** 168–82
- Fung I, John J, Lerner J, Matthews E, Prather M J, Steele L P and Fraser P J 1991 Three-dimensional model synthesis of the global methane cycle *J. Geophys. Res.* **96** 13033–65
- Gedney N and Cox P 2003 The sensitivity of global climate model simulations to the representation of soil moisture heterogeneity *J. Hydrometeorol.* **4** 1265–75
- Ghosh A *et al* 2015 Variations in global methane sources and sinks during 1910–2010 *Atmos. Chem. Phys.* **15** 2595–612
- Gloor M, Brienen R J W, Galbraith D, Feldpausch T R, Schongart J, Guyot J L, Espinoza J C, Lloyd J and Phillips O L 2013 Intensification of the Amazon hydrological cycle over the last two decades *Geophys. Res. Lett.* **40** 1–5
- Grant R F, Humphreys E R and Laflaur P 2015 Ecosystem CO<sub>2</sub> and CH<sub>4</sub> exchange in a mixed tundra and a fen within a hydrologically diverse Arctic landscape: 1. Modeling versus measurements *J. Geophys. Res. Biogeosci.* **120** 1366–87
- Gurney K R *et al* 2003 TransCom 3 CO<sub>2</sub> inversion intercomparison: 1. Annual mean control results and sensitivity to transport and prior flux information *Tellus* **55B** 555–79
- Harris I, Jones P D, Osborn T J and Lister D H 2013 Updated high-resolution grids of monthly climatic observations—the CRU TS3.10 dataset *Int. J. Climatol.* **34** 623–42

- Heimann M 2011 Enigma of the recent methane budget *Nature* **476** 157–8
- Herrero M, Havlik P, Valin H, Notenbaert A, Rufino M C, Thornton P K, Blümmel M, Weiss F, Grace D and Obersteiner M 2013 Biomass use, production, feed efficiencies, and greenhouse gas emissions from global livestock systems *Proc. Natl Acad. Sci.* **110** 20888–93
- Hess L L, Melack J M, Affonso A G, Barbosa C, Gastil-Buhl M and Novo E M L M 2015 Wetlands of the lowland amazon basin: extent, vegetative cover, and dual-season inundated area as mapped with JERS-1 synthetic aperture radar *Wetlands* **35** 745–56
- Hickler T, Smith B, Prentice I C, Mjofors K, Miller P, Arneth A and Sykes M T 2008 CO<sub>2</sub> fertilization in temperate FACE experiments not representative of boreal and tropical forests *Glob. Change Biol.* **14** 1531–42
- Hilker T, Lyapustin A I, Tucker C J, Hall F G, Myneni R B, Wang Y, Bi J, Mendes de Moura Y and Sellers P J 2014 Vegetation dynamics and rainfall sensitivity of the Amazon *Proc. Natl Acad. Sci.* **111** 16041–6
- Hodson E L, Poulter B, Zimmermann N E, Prigent C and Kaplan J O 2011 The El Niño–Southern Oscillation and wetland methane interannual variability *Geophys. Res. Lett.* **38** L08810
- Hooijer A, Page S, Canadell J G, Sivius M, Kwadijk J, Wosten H and Jauhiainen J 2010 Current and future CO<sub>2</sub> emissions from drained peatlands in Southeast Asia *Biogeosciences* **7** 1505–14
- Jackson R B, Vengosh A, Carey J W, Davies R J, Darrah T H, O’Sullivan F and Petron G 2014 The environmental costs and benefits of fracking *Ann. Rev. Environ. Resour.* **39** 327–62
- Joos F and Spahni R 2008 Rates of change in natural and anthropogenic radiative forcing over the past 20 000 years *Proc. Natl Acad. Sci. USA* **105** 1425–30
- Jung M *et al* 2010 Recent decline in the global land evapotranspiration trend due to limited moisture supply *Nature* **467** 951–4
- Kai F M, Tyler S C, Randerson J T and Blake D R 2011 Reduced methane growth rate explained by decreased Northern hemisphere microbial sources *Nature* **476** 194–7
- Kanamitsu M, Ebisuzaki W, Woollen J, Yang S K, Hnilo J J, Fiorino M and Potter G L 2002 NCEP–DEO AMIP-II reanalysis (R-2) *Bull. Am. Meteorol. Soc.* **83** 1631–43
- Kaplan J O 2002 Wetlands at the last glacial maximum: distribution and methane emissions *Geophys. Res. Lett.* **29** 3–1–3–4
- Karl T R, Arguez A, Huang B, Lawrimore J H, McMahon J R, Menne M J, Peterson T C, Vose R S and Zhang H-M 2015 Possible artifacts of data biases in the recent global surface warming hiatus *Science* **348** 1469–72
- Kirschke S *et al* 2013 Three decades of global methane sources and sinks *Nat. Geosci.* **6** 813–23
- Lara M J, McGuire A D, Euskirchen E S, Tweedie C E, Hinkel K M, Skurikhin A N, Romanovsky V E, Grosse G, Bolton W R and Genet H 2015 Polygonal tundra geomorphological change in response to warming alters future CO<sub>2</sub> and CH<sub>4</sub> flux on the Barrow Peninsula *Glob. Change Biol.* **21** 1634–51
- Lawrence D M, Koven C D, Swenson J J, Riley W J and Slater A G 2015 Permafrost thaw and resulting soil moisture changes regulate projected high-latitude CO<sub>2</sub> and CH<sub>4</sub> emissions *Environ. Res. Lett.* **10** 094011
- Le Quéré C *et al* 2015 Global carbon budget 2015 *Earth Syst. Sci. Data* **7** 349–96
- Leff B, Ramankutty N and Foley J A 2004 Geographic distribution of major crops around the world *Glob. Biogeochem. Cycles* **18** GB1009
- Lehner B and Doll P 2004 Development and validation of a global database of lakes, reservoirs and wetlands *J. Hydrol.* **296** 1–22
- Li C, Qiu J, Frolking S, Xiao X, Salas W, Moore B, Boles S, Huang Y and Sass R 2002 Reduced methane emissions from large-scale changes in water management of China’s rice paddies during 1980–2000 *Geophys. Res. Lett.* **29** 33–31–33–34
- Matthews E and Fung I 1987 Methane emission from natural wetlands: global distribution, area, and environmental characteristics of sources *Glob. Biogeochem. Cycles* **1** 61–86
- Melton J R *et al* 2013 Present state of global wetland extent and wetland methane modelling: conclusions from a model inter-comparison project (WETCHIMP) *Biogeosciences* **10** 753–88
- Meng L, Paudel R, Hess P G M and Mahowald N M 2015 Seasonal and inter-annual variability in wetland methane emissions simulated by CLM4Me0 and CAM-chem and comparisons to observations of concentrations *Biogeosciences* **12** 2161–212
- Miller S M, Commane R, Melton J R, Andrews A E, Benmergui J, Dlugokencky E J, Janssens-Maenhout G, Michalak A M, Sweeney C and Worthy D E J 2016 Evaluation of wetland methane emissions across North America using atmospheric data and inverse modeling *Biogeosciences* **13** 1329–39
- Mueller B and Zhang X 2015 Causes of drying trends in northern hemispheric land areas in reconstructed soil moisture data *Clim. Change* **134** 255–67
- Nisbet E G, Dlugokencky E J and Bousquet P 2014 Methane on the rise—again *Science* **343** 493–4
- Papa F *et al* 2015 Satellite-derived surface and sub-surface water storage in the Ganges–Brahmaputra River Basin *J. Hydrol.: Reg. Stud.* **4** 15–35
- Papa F, Prigent C, Aires F, Jimenez C, Rossow W B and Matthews E 2010 Interannual variability of surface water extent at the global scale, 1993–2004 *J. Geophys. Res.* **115** D12111
- Parmentier F J W, Zhang W, Mi Y, Zhu X, van Huissteden J, Hayes D J, Zhuang Q, Christensen N L and McGuire A D 2015 Rising methane emissions from northern wetlands associated with sea ice decline *Geophys. Res. Lett.* **42** 7214–22
- Patra P K, Saeki T, Dlugokencky E, Ishijima K, Umezawa T, Ito A, Aoki S, Morimoto S, Kort E A and Crotwell A M 2016 Regional methane emission estimation based on observed atmospheric concentrations 2002–2012 *J. Meteorol. Soc. Jpn.* **94** 91–113
- Peregon A, Maksyutov S, Kosykh N P and Mironycheva-Tokareva N P 2008 Map-based inventory of wetland biomass and net primary production in western Siberia *J. Geophys. Res.* **113** G01007
- Petrescu A M R *et al* 2015 The uncertain climate footprint of wetlands under human pressure *Proc. Natl Acad. Sci.* **112** 4594–9
- Poulter B *et al* 2015 Plant functional type classification for earth system models: results from the European Space Agency’s land cover climate change initiative *Geosci. Model Dev.* **8** 429–62
- Prather M J, Holmes C D and Hsu J 2012 Reactive greenhouse gas scenarios: systematic exploration of uncertainties and the role of atmospheric chemistry *Geophys. Res. Lett.* **39** L09803
- Prigent C, Papa F, Aires F, Rossow W B and Matthews E 2007 Global inundation dynamics inferred from multiple satellite observations, 1993–2000 *J. Geophys. Res.* **112** D12107
- Ribeiro I O, de Souza R A F, Andreoli R V, Kayano M T and Costa P S 2016 Spatiotemporal variability of methane over the Amazon from satellite observations *Adv. Atmos. Sci.* **33** 852–64
- Rice A L, Butenhoff C L, Teama D G, Roger F H, Khalil M A K and Rasmussen R A 2016 Atmospheric methane isotopic record favors fossil sources flat in 1980s and 1990s with recent increase *Proc. Natl Acad. Sci.* **113** 10791–6
- Ridgwell A J, Marshall S J and Gregson K 1999 Consumption of atmospheric methane by soils: a process-based model *Glob. Biogeochem. Cycles* **13** 59–70
- Rigby M *et al* 2008 Renewed growth of atmospheric methane *Geophys. Res. Lett.* **35** L22805
- Riley W J, Subin Z M, Lawrence D M, Swenson J J, Torn M S, Meng L, Mahowald N M and Hess P 2011 Barriers to predicting changes in global terrestrial methane fluxes: analyses using CLM4Me, a methane biogeochemistry model integrated in CESM *Biogeosciences* **8** 1925–53
- Ruddiman W F 2013 The Anthropocene *Annu. Rev. Earth Planet. Sci.* **41** 45–68
- Saunoy M *et al* 2016 The global methane budget: 2000–2012 *Earth Syst. Sci. Data Discuss.* **8** 697–751
- Schaefer H *et al* 2016 A 21st century shift from fossil-fuel to biogenic methane emissions indicated by <sup>13</sup>CH<sub>4</sub> *Science* **352** 80–84



- Schaefer K, Zhang T, Bruhwiler L and Barret A P 2011 Amount and timing of permafrost carbon release in response to climate warming *Tellus* **63B** 165–80
- Scholze M, Knorr W, Arnell N W and Prentice I C 2006 A climate-change risk analysis for world ecosystems *Proc. Natl Acad. Sci.* **103** 13116–20
- Schroeder R, McDonald K C, Chapman B D, Jensen K, Podest E, Tessler Z D, Bohn T J and Zimmermann R 2015 Development and Evaluation of a multi-year fractional surface water data set derived from active/passive microwave remote sensing data *Remote Sens.* **7** 16688–732
- Schuur E A G *et al* 2015 Climate change and the permafrost carbon feedback *Nature* **520** 171–9
- Shi X, Thornton P E, Riccuiuto D M, Hanson P J, Mao J, Sebestyen S D, Griffiths N A and Bisht G 2015 Representing northern peatland microtopography and hydrology within the community land model *Biogeosciences* **12** 3381–418
- Sjogersten S, Black C R, Evers S, Hoyos-Santillan J, Wright E L and Turner B L 2014 Tropical wetlands: a missing link in the global carbon cycle? *Glob. Biogeochem. Cycles* **28** 1371–86
- Spahni R *et al* 2011 Constraining global methane emissions and uptake by ecosystems *Biogeosciences* **8** 1643–65
- Stocker B D, Roth R, Joos F, Spahni R, Steinacher M, Zaehele S, Bouwman L, Ri X and Prentice I C 2013 Multiple greenhouse-gas feedbacks from the land biosphere under future climate change scenarios *Nat. Clim. Change* **3** 666–72
- Sweeney C *et al* 2016 No significant increase in long-term CH<sub>4</sub> emissions on North Slope of Alaska despite significant increase in air temperature *Geophys. Res. Lett.* **43** 6604–11
- Tan Z and Zhuang Q 2015 Arctic lakes are continuous methane sources to the atmosphere under warming conditions *Environ. Res. Lett.* **10** 054016
- Tian H *et al* 2016 The terrestrial biosphere as a net source of greenhouse gases to the atmosphere *Nature* **531** 225–8
- Turetsky M R *et al* 2014 A synthesis of methane emissions from 71 northern, temperate, and subtropical wetlands *Glob. Change Biol.* **20** 2183–97
- Turner A J, Jacob D J, Benmergui J, Wofsy S C, Maasackers J D, Butz A, Hasekamp O, Biraud S and Dlugokencky E 2016 A large increase in US methane emissions over the past decade inferred from satellite data and surface observations *Geophys. Res. Lett.* **43** 2218–24
- van der Werf G R, Randerson J T, Giglio L, Collatz G J, Kasibhatla P and Arellano A F 2006 Interannual variability in global biomass burning emissions from 1997–2004 *Atmos. Chem. Phys.* **6** 3423–41
- van der Werf G R, Randerson J T, Giglio L, Collatz G J, Mu M, Kasibhatla P S, Morton D C, DeFries R S, Jin Y and van Leeuwen. T T 2010 Global fire emissions and the contribution of deforestation, savanna, forest, agricultural, and peat fires 1997–2009 *Atmos. Chem. Phys.* **10** 11707–35
- Verpoorter C, Kutser T, Seekell D A and Tranvik L J 2014 A global inventory of lakes based on high-resolution satellite imagery *Geophys. Res. Lett.* **41** 6396–402
- Walter Anthony K M *et al* 2014 A shift of thermokarst lakes from carbon sources to sinks during the Holocene epoch *Nature* **511** 452–6
- Walter B P, Heimann M and Matthews E 2001 Modeling modern methane emissions from natural wetlands 1. Model description and results *J. Geophys. Res.* **106** 34189–206
- Wang X *et al* 2014 A two-fold increase of carbon cycle sensitivity to tropical temperature variations *Nature* **506** 212–5
- Wania R *et al* 2013 Present state of global wetland extent and wetland methane modeling: methodology of a model intercomparison project (WETCHIMP) *Geosci. Model Dev.* **6** 617–41
- Watts J D, Kimball J S, Bartsch A and McDonald K C 2014 Surface water inundation in the boreal-arctic: potential impacts on regional methane emissions *Environ. Res. Lett.* **9** 075001
- Wilson C, Gloor M, Gatti L V, Miller J B, Monks S A, McNorton J, Bloom A A, Basso L S and Chipperfield M P 2016 Contribution of regional sources to atmospheric methane over the Amazon Basin in 2010 and 2011 *Glob. Biogeochem. Cycles* **30** 400–20
- Wilson M, Bates P, Alsdorf D, Forsberg B, Horritt M, Melack J, Frappart F and Famiglietti J 2007 Modeling large-scale inundation of Amazonian seasonally flooded wetlands *Geophys. Res. Lett.* **34** L15404
- Wolter K and Timlin M S 1993 Monitoring ENSO in coads with a seasonally adjusted principal component index *Proc. of the 17th Climate Diagnostics Workshop (Norman, OK)* (NOAA/NMC/CAC, NSSL) pp 52–57
- Worden J *et al* 2013 El Niño, the 2006 Indonesian peat fires, and the distribution of atmospheric methane *Geophys. Res. Lett.* **40** 1–6
- Xu X, Yuan F, Hanson P J, Wulschleger S D, Thornton P E, Riley W J, Song X, Graham D E, Song C and Tian H 2016b Reviews and syntheses: four decades of modeling methane cycling in terrestrial ecosystems *Biogeosciences* **13** 3735–55
- Zhang B, Tian H, Ren W, Tao B, Lu C, Yang J, Banger K and Pan S 2016a Methane emissions from global rice fields: magnitude, spatiotemporal patterns, and environmental controls *Glob. Biogeochem. Cycles* **30** 1246–63
- Zhang K, Kimball J S, Nemani R, Running S W, Hong Y and Gourley J J and Yu Z 2015 Vegetation greening and climate change promote multidecadal rises of global land evapotranspiration *Sci. Rep.* **5** 15956
- Zhang Z, Zimmermann N E, Kaplan J O and Poulter B 2016b Modeling spatiotemporal dynamics of global wetlands: comprehensive evaluation of a new sub-grid TOPMODEL parameterization and uncertainties *Biogeosciences* **13** 1387–408
- Zhou L *et al* 2014 Widespread decline of Congo rainforest greenness in the past decade *Nature* **509** 86–90
- Zhu Q, Peng C, Chen H, Fang X, Liu J, Jiang H, Yang Y and Yang G 2015 Estimating global natural wetland methane emissions using process modelling: spatio-temporal patterns and contributions to atmospheric methane fluctuations *Glob. Ecol. Biogeogr.* **24** 959–72
- Zobler L 1986 A world soil file for global climate modeling NASA *Tech. Memo.* **87802** 32
- Zürcher S, Spahni R, Joos F, Steinacher M and Fischer H 2013 Impact of an abrupt cooling event on interglacial methane emissions in northern peatlands *Biogeosciences* **10** 1963–81